

Completely inelastic ball

T. Gilet,^{*} N. Vandewalle, and S. Dorbolo

Department of Physics B5a, GRASP, University of Liège, B-4000 Liège, Belgium

(Received 27 February 2009; revised manuscript received 24 April 2009; published 18 May 2009)

This Rapid Communication presents an analytical study of the bouncing of a completely inelastic ball on a vertically vibrated plate. The interplay of saddle-node and period-doubling bifurcations leads to an intricate structure of the bifurcation diagram with uncommon properties, such as an infinity of bifurcation cascades in a finite range of the control parameter Γ . A pseudochaotic behavior, consisting in arbitrarily long and complex periodic sequences, is observed through this generic system.

DOI: [10.1103/PhysRevE.79.055201](https://doi.org/10.1103/PhysRevE.79.055201)

PACS number(s): 05.45.-a, 45.50.-j

The bouncing of a partially elastic ball on a vertically vibrated plate is regarded as one of the simplest experiments that illustrates the main concepts of chaos theory [1]. The related model, which is considered as a standard in physics, shares many features with other discretely forced systems [2]. A number of variants of this problem have been investigated, e.g., with other bouncing objects [3–5], forcing [6–8], or geometry [9,10]. Among them, the Fermi problem [11], i.e., a particle that bounces between two parallel vibrated plates, has received particular attention due to its omnipresence in physics. The bouncing ball model has also numerous practical applications in a large variety of fields such as the ball-milling-induced amorphization [12] or the conception of vibration dampers in acoustics [13]. In neurosciences, the bouncing ball is a common experiment to test coordination abilities of humans [14,15]. Finally, the completely inelastic ball has deep implications in granular media physics [16,17]. Indeed, the important dissipation between multiple collisions ensures the effective inelasticity of granular matter and similar bifurcation diagrams are encountered [18]. Behaviors observed in the inelastic ball are also likely shared by any system involving reset mechanisms.

Luck and Mehta [19,20] have partly solved the partially and completely inelastic ball problems. Their works are based on the important assumption that the flight length of the ball is much greater than the forcing period, which is only the case for some flights (not all) at very high forcing. As detailed below, the ball may adopt two different behaviors depending on where it impacts: it may immediately bounce or instead stick on the plate until the plate acceleration is 1 g. The authors have stated that the ball always reaches the sticking region, which makes the motion periodic, although the period could be arbitrarily long. In this Rapid Communication, we fully resolve the motion of a completely inelastic ball that bounces on a vibrated plate of motion $x(t)=A \cos \omega t$, without any assumption on the flight duration. The apparently complex structures observed in the bifurcation diagram are rationalized.

Equations are made dimensionless thanks to the characteristic time $1/\omega$ and length g/ω^2 , where g is the gravity acceleration. Two dimensionless parameters are defined: the

reduced acceleration $\Gamma=A\omega^2/g \geq 1$ and the phase $\varphi=\omega t$. The ball takes off at $\varphi=\varphi_0$ with a velocity equal to the plate velocity; its position is then given by

$$x = \Gamma(\cos \varphi_0 - \cos \varphi) + \Gamma \sin \varphi_0(\varphi_0 - \varphi) - \frac{(\varphi - \varphi_0)^2}{2}. \quad (1)$$

The next impact occurs when $x(\varphi_i)=0$, the flight time is $T = \varphi_i - \varphi_0$ which satisfies

$$F \equiv \Gamma \cos \varphi_0(1 - \cos T) - \Gamma \sin \varphi_0(T - \sin T) - \frac{T^2}{2} = 0. \quad (2)$$

The ball can take off when the normal force exerted by the plate is directed upwards, which implies

$$\Gamma \cos \varphi_0 \geq 1. \quad (3)$$

We choose every trajectory to begin at the first phase φ_0 for which $\Gamma \cos \varphi_0=1$ and $\Gamma \sin \varphi_0=-\sqrt{\Gamma^2-1} < 0$. An example of trajectory is provided in Fig. 1. The ball may impact in the zone where $\Gamma \cos \varphi > 1$ and bounce instantaneously. Otherwise, it sticks on the plate until it reaches $\Gamma \cos \varphi=1$ where it takes off again, exactly as for the initial flight. Except in specific conditions that will be described below, the ball always ends up impacting in the sticking region, which therefore generates periodicity. By definition, a period- n motion involves n different flights (e.g., period-2 in Fig. 1). The sticking zone may be considered as a reset mechanism of the system: when the ball enters this zone, it forgets its past history.

The first flight time T satisfies $\Gamma=\Gamma_1(T)$, where

$$\Gamma_1(T) \equiv \sqrt{1 + \left(\frac{\frac{T^2}{2} - 1 + \cos T}{T - \sin T} \right)^2}. \quad (4)$$

It is shown to be the highest possible flight time for a given Γ since the ball takes off with the maximum achievable absolute velocity $\sqrt{\Gamma^2-1}$. The curve $\Gamma_1(T)$ is monotonically increasing, which means that $\Gamma_1(T)$ is the smallest Γ required to observe T .

In general, T may be computed numerically by solving Eq. (2) for given (Γ, φ_0) . This equation may be rewritten as a second-order polynomial equation in $\tan(\varphi_0/2)$ which al-

^{*}tristan.gilet@ulg.ac.be

Web site: <http://www.grasp.ulg.ac.be>

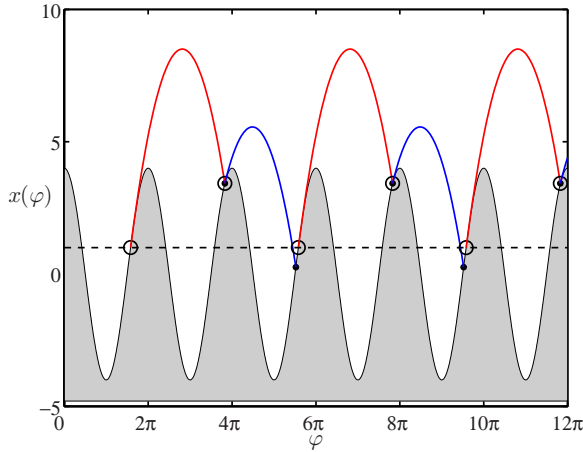


FIG. 1. (Color online) A plate is vibrated sinusoidally according to $x_p = \Gamma \cos \varphi$ (shaded). The solid line is the trajectory $x(\varphi)$ of a completely inelastic ball let on this plate when $\Gamma = 4$. The red (respectively, blue) part corresponds to the first (respectively, second) flight. The successive take-off phases φ_0 and impact phases ($\varphi_0 + T$) are represented by (○) and (●), respectively. The dashed horizontal line $x_p = \Gamma \cos \varphi = 1$ separates the bouncing and sticking zones.

ways have two solutions. Only one of them is in the $\Gamma \cos \varphi_0 \geq 1$ zone and is therefore physically relevant. In other words, there is always one and only one physical solution φ_0 corresponding to a point in the (Γ, T) diagram which satisfies $\Gamma \geq \Gamma_1(T)$; this diagram contains all the information necessary to describe the motion.

For each different successive flight i , the computed flight time is reported on the (Γ, T) diagram, where it forms a branch B_i as a function of Γ (Fig. 2). As expected, all the solutions are located below or on the curve $\Gamma = \Gamma_1(T)$, which mainly coincides with the branch B_1 except around $T = 2\pi N$,

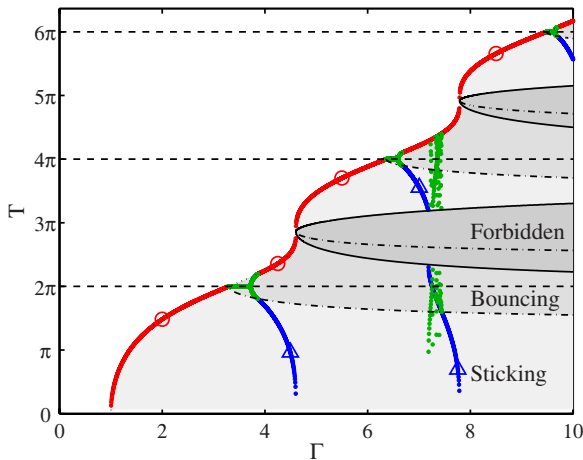


FIG. 2. (Color online) (Γ, T) diagram. Shadings indicate the different zones (bouncing, sticking, and forbidden), while colored symbol lines correspond to the branches B_i of flight i obtained by solving Eq. (2) numerically: (○) B_1 , (△) B_2 , (●) B_3 , and next ones. The dashed curve corresponds to $\Gamma_1(T)$, the decreasing solid curve corresponds to $\Gamma_{FB}(T)$, the increasing solid curve corresponds to Γ_{SF} , and the decreasing solid curve corresponds to Γ_{BS} . The dotted lines indicate fixed points in $T = 2\pi N$, with $N \in \mathbb{N}$.

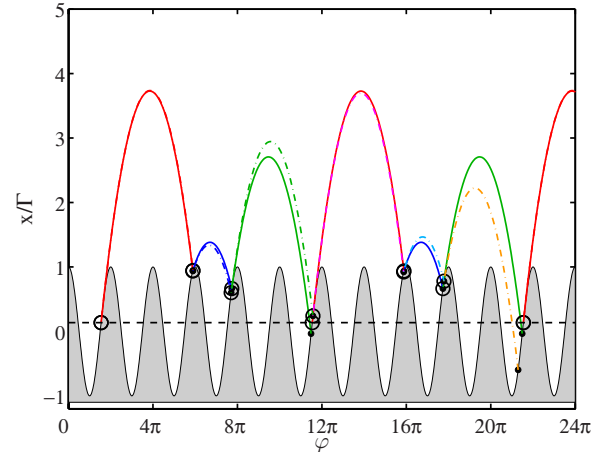


FIG. 3. (Color online) Period-doubling bifurcation. The solid trajectory ($\Gamma = 7.320$) sticks after three flights while the dash-dot trajectory ($\Gamma = 7.336$) experiences five bounces before sticking at the sixth flight. Notations are the same as in Fig. 1.

$N \in \mathbb{N}$ as explained later. The branch $B_2(\Delta)$ decreases from B_1 to zero. More than two branches are observed around $\Gamma \sim 7.3$. In the following, three kind of zones (bouncing, sticking, and forbidden) are identified in the diagram, delimited by curves $\Gamma_{BS}(T)$, $\Gamma_{FB}(T)$, and $\Gamma_{SF}(T)$. A branch that switches from a zone to another is related to a specific bifurcation of the system.

The bouncing zone corresponds to flights T that impact at a phase $\varphi_i = \varphi_0 + T$ such as $\Gamma \cos \varphi_i \geq 1$, which is equivalent to $\Gamma \geq \Gamma_{BS}(T)$,

$$\Gamma_{BS}^2 = \frac{\left(1 + \frac{T^2}{2}\right)^2 - 2\left(1 + \frac{T^2}{2}\right)(T \sin T + \cos T) + T^2 - 1}{(\sin T - T \cos T)^2}. \quad (5)$$

Since it may be shown that $d\Gamma_{BS}/dT$ has the same sign as $(1 - \Gamma \cos \varphi_0)$, only the decreasing part of Γ_{BS} is relevant as a separation between bouncing and sticking (Fig. 2). As seen in Fig. 3, a period-doubling bifurcation occurs when a branch crosses the Γ_{BS} curve from sticking to bouncing.

For some given accelerations, there is a range of flight times that cannot be experienced, as easily understood by inspecting Fig. 4. The parabolic trajectory may be tangent to the forcing sinusoid, which means that the ball smoothly lands on the vibrated plate at tangent point M . Trajectories that lay above skip this landing opportunity and impact later (after point O). On the other hand, trajectories that lay below impact and bounce before M and have a relatively short flight time T . This discontinuity in T is mainly due to the possibility for the free-flight parabola to intercept the forcing sinusoid in more than one point (only the first intersection would correspond to a physically relevant impact). This topological transition is similar to the common tangent bifurcation, which here results in incrementing or decrementing the number of flights by one. The flight time at point M is given by $\Gamma = \Gamma_{FB}(T)$, where

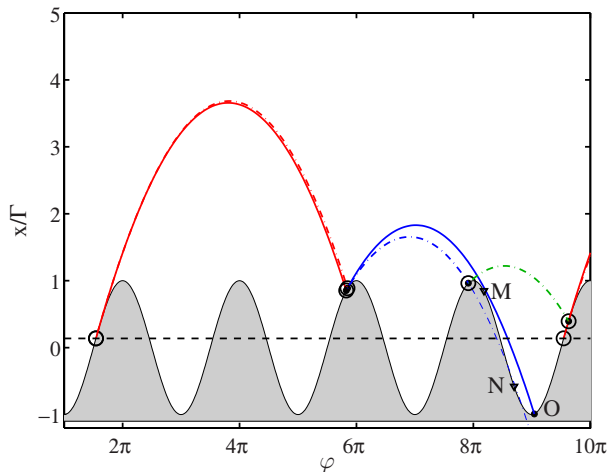


FIG. 4. (Color online) Saddle-node bifurcation. The trajectory may be tangent to the forcing sinusoid in points M and N . The solid trajectory ($\Gamma=7.15$) just passes point M , impacts in O and sticks after two flights while the dash-dot trajectory ($\Gamma=7.20$) impacts before M and so experiences three flights before sticking. Notations are the same as in Fig. 1.

$$\Gamma_{FB} = \frac{T}{2 \left| \sin^2 \frac{T}{2} \right|}. \quad (6)$$

As for Eq. (5), only the decreasing part of $\Gamma_{FB}(T)$ is physically relevant (Fig. 2). The other bound of the forbidden region $\Gamma_{SF}(T)$ is given by point O in Fig. 4, for which the position may be obtained numerically by solving Eq. (2) for $\Gamma = \Gamma_{FB}$. We note that there is another possibility for the parabola to be tangent to the sinusoid, i.e., at point N given by $T/2 = \tan^{-1} T/2, \forall \Gamma$. Nevertheless, this second tangent point cannot be reached physically.

As mentioned previously, there are some trajectories that never enter the sticking region. Nevertheless, those trajectories quickly converge to a periodic bouncing motion similar to the one encountered in the partially elastic ball [1]. A period-1 motion is obtained for $T=2\pi N$ and $\Gamma \sin \varphi_0 = -\pi N, \forall N \in \mathbb{N}_0$. In the (Γ, T) diagram (Fig. 2), the numerical solution leaves the curve $\Gamma_1(T)$ and experiences a plateau in $T=2\pi N$. This fixed point of Eq. (2) exists when $\Gamma > \sqrt{1 + \pi^2 N^2}$. At each bounce, any perturbation from this equilibrium grows by a factor equal to the Floquet multiplier

$$\frac{d(\varphi_0 + T)}{d\varphi_0} = 1 - \sqrt{\Gamma^2 - \pi^2 N^2}. \quad (7)$$

Therefore, the solution is stable when $|\frac{d(\varphi_0 + T)}{d\varphi_0}| < 1$, i.e., until $\Gamma = \sqrt{4 + \pi^2 N^2}$. Period doubling occurs for larger values of Γ . The upper branch B_1 quickly joins the Γ_1 curve, while the lower branch B_2 enters the sticking zone at the same time.

A deeper zoom in the range $\Gamma \in [7.15, 7.45]$ of the (Γ, T) diagram reveals an intricate structure (Fig. 5) generated by the successive bifurcations occurring each time a branch changes of zone. Branches of odd-degree (respectively, even) monotonically increase (decrease) with an increase in Γ . When a branch crosses one of the horizontal lines $T=2\pi N$,

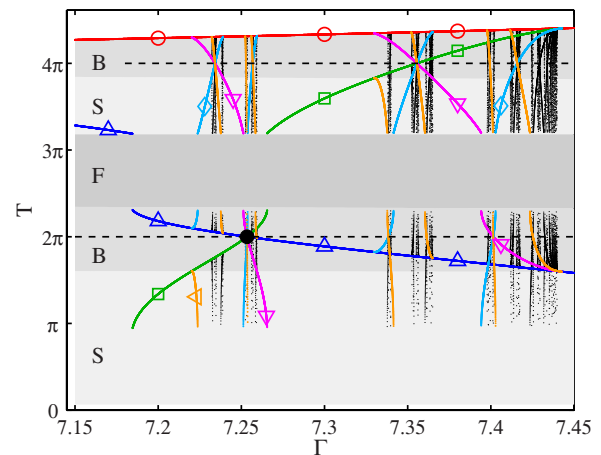


FIG. 5. (Color online) Zoom in the range $\Gamma \in [7.15, 7.45]$ of the (Γ, T) diagram. $(\circ) B_1, (\triangle) B_2, (\square) B_3, (\nabla) B_4, (\diamond) B_5, (\leftarrow) B_6$, and $(\cdot) B_i, i > 6$. The dashed lines correspond to $T=2\pi N$. The bullet (\bullet) denotes the accumulation point $\Gamma_S \approx 7.253378$, where branches $B_i, i \geq 2$ intersect each others in $T=2\pi$. Other notations are the same as in Fig. 2.

every branch of higher degree should cross the line at the same accumulation point Γ_S . This is easily understood by inspecting Fig. 6, which corresponds to acceleration very close to $\Gamma_S \approx 7.253378$: at first bounce, the ball lands in the vicinity of the unstable fixed point $T=2\pi N$. If landing is located exactly on this point, every further impact should occur at the same phase, which explains the branch crossing. But any small disturbance is amplified and the trajectory eventually reaches the sticking zone after a finite but arbitrarily large number of bounces. An infinity of branches has to be created through an infinity of bifurcations converging to the accumulation point. A second infinity of bifurcations annihilates those branches at $\Gamma \geq \Gamma_S$. A logarithmic zoom on Γ_S reveals that this cascade of bifurcations is self-similar (Fig. 7). A complex branch pattern is repeated indefinitely with a scaling factor of 30.67, different from the Feigenbaum constant. Inside this pattern, branches are seen to regularly

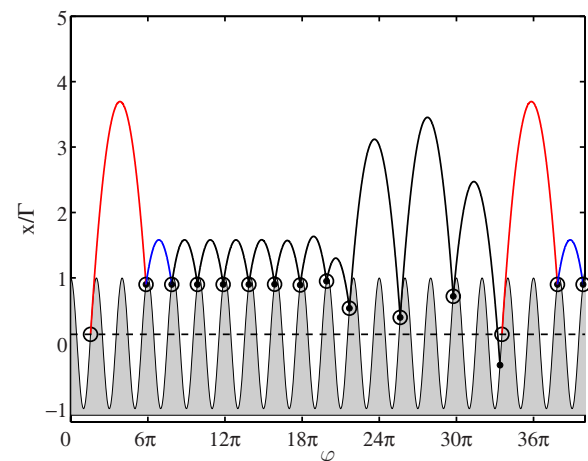


FIG. 6. (Color online) Typical trajectory that occurs when branches $B_i, i \geq 2$ enter into the vicinity of the unstable fixed point $T=2\pi$. Notations are the same as in Fig. 1.

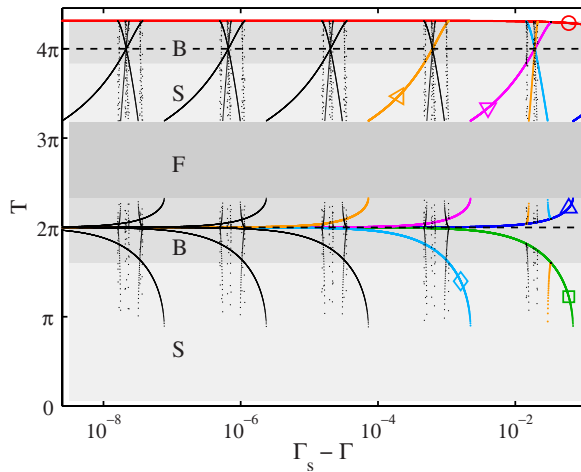


FIG. 7. (Color online) Zoom in the self-similar cascade of bifurcations converging to the accumulation point $\Gamma_s \approx 7.253\,378$. Notations are the same as in Fig. 5.

cross the $T=4\pi$ line, giving birth to infinity of other accumulation points and related bifurcation cascades. And finally, some nonconsecutive branches m and n may also intersect in other locations than $T=2\pi N$, which correspond to the unstable repetition of sequences made of $|m-n|$ different flights; a cascade of bifurcations is also related to each of

those intersections. The resulting branch structure observed in the range $\Gamma \in [7.18, 7.44]$ (Fig. 5) is thus an infinitely complex object; denumerability of the occurring bifurcations is still an open question. However, trajectories never become chaotic and, *stricto sensu*, the Lyapunov exponent is negative on each periodic solution: sufficiently small perturbations, either on the initial condition φ_0 or on the forcing parameter Γ , quickly vanish and do not qualitatively modify the trajectory. Conversely, a highly sensitive dependence on initial conditions and parameters is observed when finite perturbations are considered.

In conclusion, this Rapid Communication presents an analytical solution of the inelastic ball bouncing on a vibrated plate. Different zones are identified on the (Γ, T) diagram, transitions between them are related to tangent and period-doubling bifurcations. An infinity of bifurcation cascades is observed in a finite range $\Gamma \in [7.18, 7.44]$, leading to an intricate structure of the bifurcation diagram, although trajectories never become strictly chaotic.

T.G. and S.D. thank FRIA/FNRS for financial support. We gratefully acknowledge M. Guilmet, R. Sepulchre, and H. Croisier for fruitful discussions. This project was a part of IAP-P6/17 from the Belgian Science Policy and COST-P21 actions.

-
- [1] N. B. Tufillaro, T. Abbott, and J. P. Reilly, *An Experimental Approach to Nonlinear Dynamics and Chaos* (Addison-Wesley, Reading, MA, 1992).
- [2] R. B. Davis and L. N. Virgin, *Int. J. Non-linear Mech.* **42**, 744 (2007).
- [3] S. Dorbolo, D. Volfson, L. Tsimring, and A. Kudrolli, *Phys. Rev. Lett.* **95**, 044101 (2005).
- [4] A. Kudrolli, G. Lumay, D. Volfson, and L. S. Tsimring, *Phys. Rev. Lett.* **100**, 058001 (2008).
- [5] T. Gilet and J. W. M. Bush, *Phys. Rev. Lett.* **102**, 014501 (2009).
- [6] G. A. Luna-Acosta, *Phys. Rev. A* **42**, 7155 (1990).
- [7] S. N. Majumdar and M. J. Kearney, *Phys. Rev. E* **76**, 031130 (2007).
- [8] E. D. Leonel and M. R. Silva, *J. Phys. A: Math. Theor.* **41**, 015104 (2008).
- [9] Y. Fang, M. Gao, J. J. Wylie, and Q. Zhang, *Phys. Rev. E* **77**, 041302 (2008).
- [10] V. Milner, J. L. Hanssen, W. C. Campbell, and M. G. Raizen, *Phys. Rev. Lett.* **86**, 1514 (2001).
- [11] E. Fermi, *Phys. Rev.* **75**, 1169 (1949).
- [12] Y. Chen, M. Bibole, R. Le Hazif, and G. Martin, *Phys. Rev. B* **48**, 14 (1993).
- [13] S. Ramachandran and G. Lesieutre, *J. Vibr. Acoust.* **130**, 021008 (2008).
- [14] H. Katsumata, V. Zatsiorsky, and D. Sternad, *Exp. Brain Res.* **149**, 17 (2003).
- [15] R. Ronsse, P. Lefèvre, and R. Sepulchre, *Neural Networks* **21**, 577 (2008).
- [16] F. Melo, P. B. Umbanhowar, and H. L. Swinney, *Phys. Rev. Lett.* **75**, 3838 (1995).
- [17] I. S. Aranson and L. S. Tsimring, *Rev. Mod. Phys.* **78**, 641 (2006).
- [18] J. M. Pastor, D. Maza, I. Zuriguel, A. Garcimartín, and J.-F. Boudet, *Physica D* **232**, 128 (2007).
- [19] A. Mehta and J. M. Luck, *Phys. Rev. Lett.* **65**, 393 (1990).
- [20] J. M. Luck and A. Mehta, *Phys. Rev. E* **48**, 3988 (1993).